Enhanced α decays to negative-parity states in even-even nuclei with octupole deformation

W. M. Seif,[1,2,*] A. Adel,[1,†] N. V. Antonenko,[3] and G. G. Adamian[3]
[1]*Cairo University, Faculty of Science, Department of Physics, 12613 Giza, Egypt*
[2]*Cairo University, Faculty of Postgraduate studies for Nanotechnology, Sheikh-Zayed, 12588 Giza, Egypt*
[3]*Joint Institute for Nuclear Research, 141980 Dubna, Russia*

(Received 26 January 2023; accepted 17 March 2023; published 5 April 2023)

The α decays of even-even Ra, Th, U, and Pu isotopes to ground and excited states of daughter nuclei with neutron numbers of $N = 130$–140 are investigated. These nuclei show some enhanced α-branching ratios to negative-parity states (1^-, 3^-), compared with the decays to positive-parity states (4^+) of comparable energy. This enhancement correlates with appearance of static octupole deformation, rather than spherical nuclear shapes or dynamic asymmetric vibrational states. The highly enhanced branching ratios occur for α decays to the 1^- and 3^- states of the Ra isotopes with $N = 134$, 136, 138, then to 1^- state in Th ($N = 134$–140) and to the 3^- state in Rn ($N = 132$–136) isotopes.

DOI: 10.1103/PhysRevC.107.044601

I. INTRODUCTION

The low-lying negative-parity states and static octupole shapes were observed in Ra and Th isotopes with neutron numbers around $N = 134$. Similar behavior of the 1^- and 3^- states was indicated in the lanthanide and actinide regions of $Z = 56$–82 ($N = 86$–88) and $Z = 82$–94 ($N = 130$–134) [1]. Generally, the transition from spherical shapes and dynamic vibrations to static asymmetric deformed shapes requires the investigation of nuclear structure in the region of $Z \approx 88$ and $N \approx 132$. In this region, the octupole coupling between orbitals around the Fermi surface determines the intrinsic shape [2,3]. Considering ^{222}Ra as a pear shape (nucleus with static octupole deformation) and ^{228}Ra as an octupole vibrator, one can explain the observed behavior of $E3$ matrix elements of different nuclear transitions [4]. The presence of low-lying bands of negative-parity in even-even nuclei in this mass region is a signature for reflection asymmetry about the plane perpendicular to the corresponding symmetry axis. This reflection asymmetry could be also due to molecular states of α clusters in these nuclei [5].

The static octupole deformation is considered to be the extreme case of the asymmetric vibrational and rotational octupole collectivity of deformed nuclei. The reflection-asymmetric octupole deformation is experimentally and theoretically indicated for a few tens of actinides of $A = 218$–229 [6,7], within the close lying neutron ($\nu g_{9/2}$ and $\nu j_{15/2}$) and proton ($\pi f_{7/2}$ and $\pi i_{13/2}$) orbitals. Also, a group of statically octupole deformed nuclei has been observed in the lanthanide mass regions of $A = 144$–155 [7]. For such nuclei, the deviation between the experimentally observed quantities and their theoretical values had been minimized upon taking into account the octupole correlations. This includes their masses [8], structure [4,9,10], and reactions [11–20]. This is clearly reflected in the structure of nuclei of low-lying negative-parity states. Even though the octupole reflection-asymmetric shapes are not as stable as the quadrupole and hexadecapole symmetric deformations, they influence the band structure and its properties. For example, the shift between the centers of charge and mass in the presence of reflection-asymmetric deformations may cause dipole moment to be arisen in the intrinsic frame [6]. Moreover, the asymmetric mass distribution of a fissioning nucleus puts its finger on its fission mass distributions. For instance, fission resonances due to reflection-asymmetric hyperdeformed shapes have been measured in Th and U nuclei [21,22].

Generally, both the static octupole deformation and the dynamical octupole vibrations impact the structure-related spectroscopic properties [4,9,23,24], as well as the height, position, and curvature of the Coulomb barrier between interacting nuclei [12,13,25,26]. This in turn enhances the fusion cross section at sub- and near-barrier energies [19,20,27,28]. It influences also the nuclear decays [29–33], determining the corresponding optimum orientations. α decay becomes more complex for deformed emitters due to the fact that both the ground state and low-lying excited states of the daughter nuclei are available for α transitions. Additionally, the decay channels of these states are strongly coupled during the tunneling process [34–36]. In some cases the presence of the octupole deformation cancel the effect of the other deformations bringing the fusion barrier back to the spherical case [15,17]. As found, the values of hindrance factor for α decay to the 1^- level in the Rn and Ra isotopes decrease with N [14]. It becomes close to unity for $N \leqslant 136$ [37]. This has been attributed to the switch of the structure from low-lying dynamic vibrational states of negative-parity into static octupole deformation [2]. All that was mentioned above motivated us to precisely investigate the α-decay modes to

*wseif@sci.cu.edu.eg
†ahmed_adel@cu.edu.eg, ahmedadel@sci.cu.edu.eg

the negative-parity states in even-even nuclei, in the region around $N = 136$. Our aim is to demonstrate the correlation between static octupole deformation and enhanced α decays to negative parity states.

II. THEORETICAL FRAMEWORK

During the α-decay fine structure, α transitions could proceed to the ground state (g.s.) as well as to the different excited daughter states. If the daughter nucleus is in the excited state i, the Q value must be reduced by the excitation energy, E_i^*, from the Q value of the g.s. to g.s. transition ($Q_{\text{g.s.}\to\text{g.s.}}$), as [38,39]

$$Q_i = Q_{\text{g.s.}\to\text{g.s.}} - E_i^*. \tag{1}$$

The conservation of angular momentum and parity in the α-decay process limits the number of feasible transitions to daughter nucleus states that can be populated, as well as their intensities according to the following spin-parity selection rule [40]:

$$|J - J_i| \leqslant \ell \leqslant |J + J_i| \quad \text{and} \quad \frac{\pi_i}{\pi} = (-1)^\ell, \tag{2}$$

where J and J_i are the spins of the parent and the daughter nuclei, respectively, in the state i, and π and π_i are their corresponding parities. Favored α transitions are among the most popular, connecting states with the same spin and parity in which the orbital angular momentum carried by the α particle vanishes [38]. Unfavored transitions, on the other hand, occur when the emission states have different spin and parity assignments than the daughter states and the α particle carries nonzero orbital angular momentum [41–43].

The total decay width, Γ, is then calculated as

$$\Gamma = \sum_\ell \Gamma_\ell = \sum_\ell \frac{\hbar}{2} \int_0^\pi d\theta \, \nu_{\alpha\ell}(\theta) P_{\alpha\ell}(\theta) \, S_{\alpha\ell}, \tag{3}$$

where the assault frequency $\nu_{\alpha\ell}$ and penetration probability $P_{\alpha\ell}$ depend on emission angle θ in the case of deformed daughter nucleus. The integration over θ is required to obtain the total decay width [44,45]. The spectroscopic factor $S_{\alpha\ell}$ is related to the probability to form an α particle on nuclear surface with angular momentum ℓ. So the multipole expansion of nuclear surface defines the set of ℓ in Eq. (3). The odd ℓ appear in Eq. (3) if the daughter nucleus has octupole deformation [31,46].

We assume that a spherical α particle interacts with a deformed daughter nucleus that is axially symmetric. At a certain emission angle θ, the assault frequency is

$$\nu_{\alpha\ell}(\theta) = \left[\int_{R_1(\theta)}^{R_2(\theta)} \frac{2\mu}{\hbar k(r,\theta)} \, dr \right]^{-1}, \tag{4}$$

and the penetration probability is calculated within the Wentzel-Kramers-Brillouin (WKB) approximation [44] as

$$P_{\alpha\ell}(\theta) = \exp\left(-2 \int_{R_2(\theta)}^{R_3(\theta)} k(r,\theta) \, dr \right), \tag{5}$$

where $k(r,\theta) = \sqrt{2\mu |V_T(r,\theta) - Q_\alpha|/\hbar^2}$ is the wave number and $R_i (i = 1, 2, 3)$ are the three orientation-dependent classical turning points at which $V_T(r,\theta)|_{r=R_i} = Q_\alpha$.

The α-decay half-life is related to the decay width Γ as [44,47]

$$T_{1/2} = \frac{\hbar \ln 2}{\Gamma}. \tag{6}$$

The spectroscopic factor $S_{\alpha\ell}$ is related to the square of the amplitude in the multipole expansion of the wave function of the relative motion of an α particle on the nuclear surface. The microscopic calculation of $S_{\alpha\ell}$ is cumbersome and requires a number of assumptions [48]. So, at the first stage, it is desirable to use a phenomenological method to evaluate $S_{\alpha\ell}$. For even-even nuclei considered, the spectroscopic factor for the parent nucleus $A(N, Z)$ can be estimated, in terms of the numbers of neutrons $(N - N_0)$ and protons $(Z - Z_0)$ outside the corresponding shell/subshell closures (Z_0, N_0), using the semiempirical formula given by [29,31,49,50]

$$S_{\alpha\ell} = \mathcal{A}[e^{-0.003(Z-Z_0-Z_c)^2 - 0.006(N-N_0-N_c)^2}] H_\ell \tag{7}$$

with the hindrance (H_ℓ) factor given as

$$H_\ell = e^{1-n-0.6\ell}. \tag{8}$$

This expression accounts for the hindrance of the unfavored α-decay modes to daughter states of different spin than that of the parent nucleus. In Eq. (8), n defines the order of the duplicated daughter states of the same spin-parity (J^π) [49], in which the daughter nucleus is produced. As clearly seen in Eq. (8), H_ℓ gradually decreases with increasing both the state order (n) and the difference in spin (ΔJ) between the parent and daughter states, which appears in increasing the orbital angular momentum carried by the α particle (ℓ). This indicates more hindrance for such transitions, where the decay slows down compared with the corresponding favored decay modes between states of identical spin-parity. The hindrance is expected to increase for the odd values of ℓ, which indicate a change in parity from parent to daughter nuclei [43], than for the even values. Using Eq. (7), one can satisfactory reproduce the experimentally extracted preformation probability for the favored and unfavored α decays to different states of the daughter nucleus [29,31,49,50]. For the α emitters of shell closures $Z_0 = 82$ and $N_0 = 126$, we have $\mathcal{A}(Z_C = N_C = 12) = 0.105$ [31,51,52]. The values of Z_c and N_c define the intershell numbers of protons and neutrons that yield local maximum of S_α. The fitting parameters of Eq. (7) are obtained from extensive studies of huge decay data along the whole nuclear chart.

The total interaction potential between the α-particle and daughter nucleus is given by [49]

$$V_T(r,\theta) = \lambda(\theta) V_N(r,\theta) + V_C(r,\theta) + \frac{\hbar^2}{2\mu} \frac{\ell(\ell+1)}{r^2}, \tag{9}$$

where $\lambda(\theta)$ is the renormalization factor of the nuclear potential which is determined by applying the Bohr-Sommerfeld quantization condition [44,45,53,54]. V_C and V_N represent the attractive nuclear and repulsive Coulomb parts of the

potential, respectively. The last term in Eq. (9) represents the centrifugal part of the potential.

To compute the nuclear part of the potential, we will use the Hamiltonian energy density formalism [55] based on the Skyrme–SLy4 [56] NN interaction. The nuclear interaction potential is defined in this method as the difference between the whole system's energy expectation value E determined at a finite separation distance r and at infinity [43,57],

$$\begin{aligned} V_N(r,\theta) &= E(r) - E(\infty) \\ &= \int \{\mathcal{H}[\rho_{p\alpha}(\vec{x}) + \rho_{pD}(r,\vec{x},\theta), \rho_{n\alpha}(\vec{x}) \\ &\quad + \rho_{nD}(r,\vec{x},\theta)] - \mathcal{H}_\alpha[\rho_{p\alpha}(\vec{x}), \rho_{n\alpha}(\vec{x})] \\ &\quad - \mathcal{H}_D[\rho_{pD}(\vec{x}), \rho_{nD}(\vec{x})]\} d\vec{x}, \end{aligned} \tag{10}$$

where $\mathcal{H}$, $\mathcal{H}_\alpha$, and $\mathcal{H}_D$ represent the Skyrme energy density functionals of the composite system, α particle, and the daughter nucleus (D), respectively. $\rho_{ij}(i = p, n \text{ and } j = \alpha, D)$ are the density distributions of the protons (p) and neutrons (n) associated to α and daughter (D) nuclei. The energy density functional $\mathcal{H}$ is given by [56–58]

$$\begin{aligned} \mathcal{H}\big(\rho_i, \tau_i, \vec{J}_i\big) &= \frac{\hbar^2}{2m} \sum_{i=n,p} \tau_i(\rho_i, \vec{\nabla}\rho_i, \nabla^2\rho_i) \\ &\quad + \mathcal{H}_{\text{Sky}}(\rho_i, \tau_i, \vec{J}_i) + \mathcal{H}_C^{\text{exch}}(\rho_p), \end{aligned} \tag{11}$$

where $\tau_{i=p,n}$ and $\vec{J}_{i=p,n}$ define, respectively, the kinetic energy and the spin-orbit densities. The explicit representations of the nuclear ($\mathcal{H}_{\text{Sky}}$) and the exchange Coulomb ($\mathcal{H}_C^{\text{exch}}$) energy density functionals are provided in Refs. [29,43,56,57].

The double-folding model will be used to determine the direct Coulomb part of the interaction potential as [45,47,49]

$$V_C(r,\theta) = \int d\vec{r}_1 \int d\vec{r}_2 \frac{e^2}{|\vec{r} + \vec{r}_2 - \vec{r}_1|} \rho_{p\alpha}(\vec{r}_1)\rho_{pD}(\vec{r}_2). \tag{12}$$

The density distribution of the α particle is to be of standard Gaussian form, $\rho_\alpha(r) = 0.4229\exp(-0.7024r^2)$. The two-parameter Fermi shape can be used to calculate the proton and neutron density distributions of deformed daughter nuclei as

$$\rho_{n(p)}(r,\vartheta) = \rho_{0n(p)}\big(1 + e^{[r - R_{n(p)}(\vartheta)]/a_{n(p)}}\big)^{-1}. \tag{13}$$

The half-density radii can be written as an expansion in spherical harmonics with different multipole deformation parameters $\beta_i(i = 2, 3, 4, 6)$ [8], ϑ is the deformed nucleus's polar angle with respect to its symmetry axis

$$R_{n(p)}(\vartheta) = R_{0n(p)}\left[1 + \sum_{i=2,3,4,6} \beta_i Y_{i0}(\vartheta)\right]. \tag{14}$$

For reliable determination of the neutron and proton density distributions, we use the following formulas for radii $R_{0n(p)}$ and diffuseness $a_{n(p)}$ according to Ref. [59] which are in good agreement with the full Hartree-Fock (HF) calculations and the available experimental data:

$$\begin{aligned} R_{0n} &= 0.953\,N^{1/3} + 0.015\,Z + 0.774, \\ R_{0p} &= 1.322\,Z^{1/3} + 0.007\,N + 0.022, \\ a_n &= 0.446 + 0.072\left(\frac{N}{Z}\right), \\ a_p &= 0.449 + 0.071\left(\frac{Z}{N}\right). \end{aligned} \tag{15}$$

III. RESULTS AND DISCUSSION

Here, we study the α decays from the ground state of even-even actinides to the ground and excited states of their daughter nuclei. Figures 1(a)–1(c) show the branching ratio of α-decay modes from even-even $^{216\text{–}226}$Ra, $^{218\text{–}232}$Th, and $^{222\text{–}238}$U isotopes to different states of their $^{212\text{–}222}$Rn, $^{214\text{–}228}$Ra, and $^{218\text{–}234}$Th daughter nuclei, respectively. All these isotopes have exact or almost 100% total intensity of α decay, and their daughters have neutron numbers N_d = 126–140. As expected, in Fig. 1 the major fraction of the α-branching ratio appear for the decays to the ground 0^+ state then to the first 2^+ state. Decays to the lowest 1^- and 3^- states occur with relatively high intensity for the isotopes producing daughter nuclei with even N_d = 130–138. The largest intensity (about 1%) to negative-parity states is obtained for the α decays to ^{220,222}Ra (N_d = 132, 134) and ^{224}Th (N_d = 134) daughter isotopes. There is intensity of the order of 10^{-1} for the α decays resulting in the negative-parity states of ^{220,222,224}Ra (N_d = 132, 134, 136) and ^{226}Th (N_d = 136) isotopes. Also a non-negligible intensity (about 10^{-2}%) is obtained for α decays to negative-parity states of ^{218,224,226}Ra (N_d = 130, 136, 138) and ^{226,228}Th (N_d = 136, 138). Thus, the relative enhanced α decays to negative-parity states frequently appear in the α decays leading to N_d = 132, 134, and 136, and with a little enhanced intensity for the decays leading to N_d = 130 and 138. Moreover, the largest number of partial decay modes to various states of the daughter nuclei appears for N_d = 130–140.

The branching ratio as a function of the state energy is displayed in Fig. 1(d) for even-even $^{222\text{–}230}$Th isotopes, which show α-decay modes to negative-parity states of daughter nuclei with N_d = 130–138. Figure 1(d) shows that the branching ratios to the negative-parity states (1^-, 3^-, 5^-) confirm the expected inverse behavior of B_α with the state energy E_{ex}. At close state energies, the α decays to negative-parity states in some isotopes show enhanced B_α with respect to those observed for the decays to positive-parity states (4^+ and 6^+) in other isotopes.

Figure 2 shows the branching ratio of the partial decay modes of the Ra, Th, and U isotopes to the asymmetric 1^- and 3^- states of their daughter nuclei which have a number of neutrons N = 132–140, relative to the corresponding branching ratio to the symmetric 4^+ states. As seen in Fig. 2, the larger branching ratios to the negative-parity states 1^- and 3^- are obtained for the decays leading to Ra (N_d = 134, 136, 138) isotopes. Coming next are the partial decays to 1^- state in Th (N_d = 134–140) then in Rn (N = 134,136) isotopes, or to the 3^- state in Rn (N_d = 132–136) then in Th (N_d = 136, 138) isotopes. As assumed, this behavior is consistent with the evolution of static octupole deformations in actinides [14,60–71]. For instance, based on covariant energy density functionals, the evolution of the topology of the potential energy

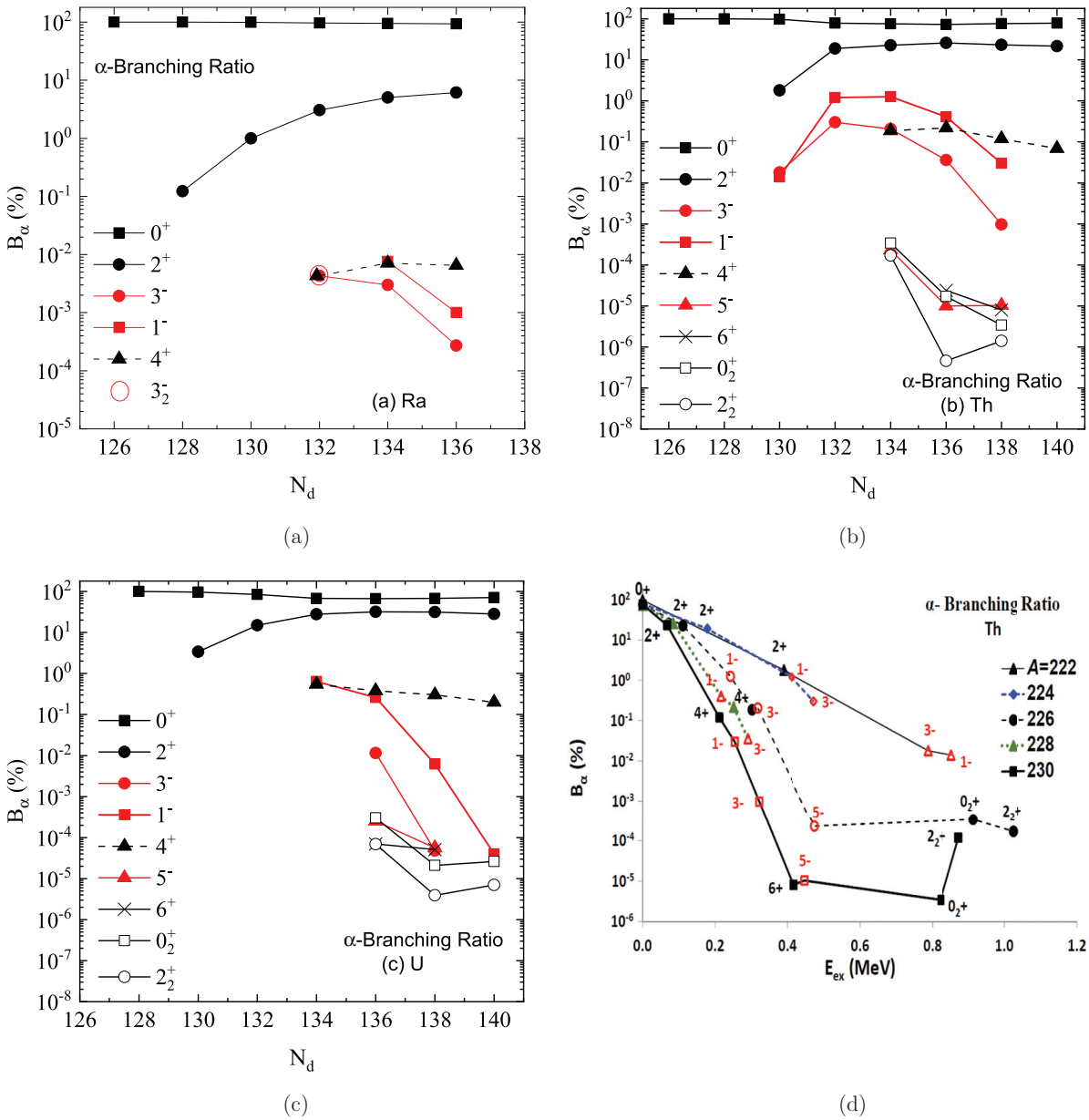

FIG. 1. The variation of α-branching ratio with the neutron number N_d of daughter nuclei for (a) Ra isotopes, (b) Th isotopes, (c) U isotopes. (d) The variation of α-branching ratio with the excitation energy E_{ex} in Th isotopes.

surfaces (PES) of the Ra and Th isotopes have shown that the energy minima associated with static octupole deformations start to appear in their isotopes with $N \geqslant 134$ [60]. The well-pronounced minima are obtained at $N = 136$ and 138. The potential energy surfaces become soft in octupole direction after $N = 138$ (Ra) and 140 (Th). The maximum contribution in binding energy due to octupole deformation is obtained at $N \approx 136$ and 138. More softer PES versus octupole deformation were obtained for the ^{222,224}Rn ($N =$ 136,138) isotopes relative to the ^{220}Rn, Ra, and Th isotopes [60]. The extracted electric octupole moments and transition strengths have shown that ^{224,226}Ra [63] have stronger octupole collectivity than ^{224}Rn and ^{230,232}Th [72,73], with clear evidences for strong static octupole deformation. Using multinucleon transfer spectroscopy, ^{222,224,226}Ra and ^{224,226}Th were also indicated as well octupole-deformed rotors at low frequencies [69]. The neighboring ^{220,228}Ra and $^{222,228–234}$Th isotopes were suggested to be octupole-vibrational nuclei at low frequencies, while at higher rotational frequencies they possess induced stable octupole deformation before turning back to reflection-symmetric shapes [69]. Also, different macroscopic-microscopic calculations have indicated $^{218–222}$Rn [67], $^{222–224}$Rn [71], and ^{220}Rn [65] to be the most Rn isotopes having octupole deformation with non-negligible gain in the binding energy due to octupole deformation, which is less than that of mentioned Ra and Th isotopes.

It is interesting to examine the influences of both the energy and the orbital angular momentum ℓ on the enhanced branching ratio of the decays to the lowest negative-parity states in even-even daughter nuclei comparing with those

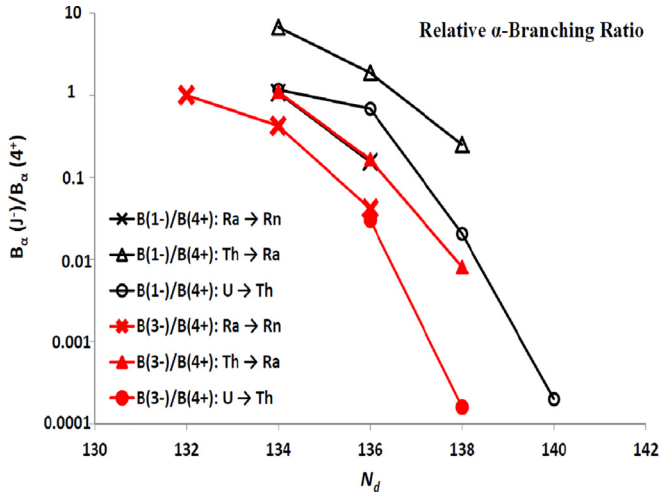

FIG. 2. The variation of the ratios of branching ratios for α decays of Ra, Th, and U isotopes to the negative-parity states 1^- and 3^- of their daughter nuclei with neutron numbers $N_d = 132$–140 and those to the 4^+ states.

corresponding to positive-parity states. Figure 3 displays the calculated partial half-life against α-decay modes from the ground state of the ^{226}Th parent nucleus to the 1^- ($Q_\alpha = 0.242$ MeV, $T_\alpha = 1.46 \times 10^5$ s) and the 4^+ (0.301 MeV, 9.81×10^5 s) states of its ^{222}Ra daughter nucleus, as a function of the transferred orbital angular momentum ℓ. The partial half-live for each decay mode is calculated at its released energy, and at the released energy corresponding to the other mode. The calculations based on the correct Q_α and ℓ_α exactly reproduce the experimental $T_\alpha(4^+)$, but result in rather small $T_\alpha(1^-)$ relative to its observed value. This is due to the additional hindrance for the decay modes between states of different parity [43] which is not in Eq. (8) and requires microscopic consideration. As clearly seen in Fig. 3, the partial

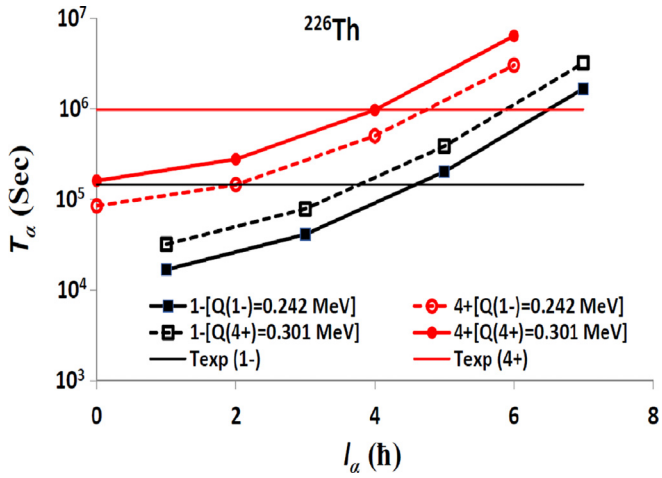

FIG. 3. The variation of the partial α-decay half-lives T_α ($0^+ \to 1^-$) and T_α ($0^+ \to 4^+$) of ^{226}Th, with the orbital angular momentum ($\ell_\alpha\hbar$), transferred by the α particle, at two energies [$Q_\alpha(1^-) = 0.242$ MeV and $Q_\alpha(4^+) = 0.301$ MeV] for both of them. The horizontal lines represent the observed T_α ($0^+ \to 1^-$) and T_α ($0^+ \to 4^+$).

T_α increases with increasing ℓ and decreases with increasing released energy. If the energies of the 1^- and 4^+ states would be the same ($Q_\alpha = 0.242$ MeV), the calculated $T_\alpha(0^+ \to 4^+)$ remains larger than the experimental values of $T_\alpha(0^+ \to 1^-)$. Thus, the enhancement for the decay mode to the 1^- state relative to the 4^+ cannot be explained only by the difference in the energies of the states 1^- and 4^+. The influence of the value of ℓ becomes important in this case. The appearance of this enhancement is related to the octupole deformation of daughter nucleus pushing down the lowest 1^- state.

Table I displays the comparison of the calculated branching ratios for the observed α decays from the ground states of even-even $^{222-232}$Th to the ground state as well as to the low-lying excited states of their even-even $^{218-228}$Ra daughter nuclei. The third and fourth columns on Table I list, respectively, the excitation energies E_{ex} (MeV) and the experimental Q_α (MeV) values for the mentioned decay channels [74]. The experimental α-decay branching ratios are reported in the fifth column. The octupole deformation β_3 is taken into account beside $\beta_{2,4,6}$ in the calculations listed in the last two columns of Table I, with and without including H_ℓ, respectively. This hindrance factor reduces the spectroscopic factor for the decays to various excited states of the daughter nucleus with $\ell > 0$.

For the Th isotopes presented in Table I, the total sum of the observed branching ratios for the α decays to excited states of daughter nuclei is about 20%, with a fraction of about 97% for the decays to positive-parity states and about 3% the α decays to negative-parity states. Generally, the estimated branching ratio for the α decays to negative-parity states slightly increases with octupole deformation β_3. The minimum standard deviations, $\sigma = \sqrt{\sum_{i=1}^{n}[\log_{10}(B_i^{\rm cal}/B_i^{\rm exp})]^2/(n-1)}$, for the calculated branching ratios for various daughter states and for the negative-parity daughter states, relative to the experimentally observed values are obtained upon including the hindrance factor of unfavored decays.

In Table II, we show the comparison between the observed and calculated α-branching ratios for the decays to different daughter states from ^{222,224,226}Ra ($N = 134, 136, 138$), ^{228,232}U ($N = 136, 140$), and ^{230}Pu ($N = 136$). The daughters of these α emitters are octupole deformed [8]. The calculations in Table II are performed considering the octupole deformations, with and without considering the hindrance factor. The spin-parity assignments of the daughter states to which the α decay occurs from the ground state of parent nucleus, the energies of the involved states, and the corresponding Q_α values are listed in columns 2, 3, and 4, respectively. As seen, there is satisfactory description of the experimental branching ratios for the decays to the states of positive and negative parity, with standard deviations of 0.672 and 1.187, respectively, upon including the hindrance factors in the α spectroscopic factor.

IV. SUMMARY AND CONCLUSIONS

We studied the α-decay modes to ground and to excited states of even(Z)-even(N) actinides, which produce daughters having neutron numbers of $N_d = 126$–140. A clear

TABLE I. Comparison of the calculated (B.R. calc) and experimental (B.R. exp) branching ratios. The calculated branching ratios are presented with and without the inclusion of the hindrance factor (H_ℓ). The octupole deformations (β_3) of daughter nuclei are taken from [8].

Parent	Transition	E_{ex} (MeV)	Q_α (MeV)	B.R. exp (%)	β_3	B.R. calc (%)	
						with H_ℓ	without H_ℓ
^{222}Th	$0^+ \to 0^+$	0	8.1270	9.82×10^{1}	−0.125	9.89×10^{1}	9.66×10^{1}
	$0^+ \to 2^+$	0.3895	7.7375	1.80×10^{0}		9.80×10^{-1}	3.17×10^{0}
	$0^+ \to (3^-)$	0.7900	7.3370	1.80×10^{-2}		1.21×10^{-2}	7.19×10^{-2}
	$0^+ \to (1^-)$	0.8530	7.2740	1.40×10^{-2}		6.09×10^{-2}	1.08×10^{-1}
^{224}Th	$0^+ \to 0^+$	0	7.2980	7.94×10^{1}	−0.127	9.51×10^{1}	8.66×10^{1}
	$0^+ \to 2^+$	0.1784	7.1196	1.91×10^{1}		3.66×10^{0}	1.11×10^{1}
	$0^+ \to (1^-)$	0.4129	6.8851	1.21×10^{0}		1.17×10^{0}	1.93×10^{0}
	$0^+ \to (3^-)$	0.4741	6.8239	3.02×10^{-1}		8.11×10^{-2}	4.46×10^{-1}
^{226}Th	$0^+ \to 0^+$	0	6.4509	7.55×10^{1}	−0.141	9.14×10^{1}	7.87×10^{1}
	$0^+ \to 2^+$	0.1111	6.3398	2.28×10^{1}		5.09×10^{0}	1.46×10^{1}
	$0^+ \to 1^-$	0.2421	6.2088	1.26×10^{0}		3.30×10^{0}	5.18×10^{0}
	$0^+ \to 4^+$	0.3014	6.1495	1.87×10^{-1}		5.74×10^{-2}	5.45×10^{-1}
	$0^+ \to 3^-$	0.3173	6.1336	2.06×10^{-1}		1.79×10^{-1}	9.33×10^{-1}
	$0^+ \to (5^-)$	0.4738	5.9771	2.30×10^{-4}		1.88×10^{-3}	3.26×10^{-2}
	$0^+ \to (0^+)$	0.914	5.5369	3.40×10^{-4}		9.70×10^{-4}	2.27×10^{-3}
	$0^+ \to 2^+$	1.0249	5.4260	1.70×10^{-4}		3.91×10^{-5}	3.04×10^{-4}
^{228}Th	$0^+ \to 0^+$	0	5.52008	7.34×10^{1}	−0.139	9.22×10^{1}	8.01×10^{1}
	$0^+ \to 2^+$	0.0844	5.43568	2.60×10^{1}		5.30	1.52×10^{1}
	$0^+ \to 1^-$	0.2160	5.30408	4.07×10^{-1}		2.35	3.72
	$0^+ \to 4^+$	0.2508	5.26928	2.18×10^{-1}		4.62×10^{-2}	4.42×10^{-1}
	$0^+ \to 3^-$	0.2903	5.22978	3.59×10^{-2}		1.0×10^{-1}	5.27×10^{-1}
^{230}Th	$0^+ \to 0^+$	0	4.7700	7.65×10^{1}	−0.112	9.40×10^{1}	8.30×10^{1}
	$0^+ \to 2^+$	0.0677	4.7023	2.34×10^{1}		5.32	1.56×10^{1}
	$0^+ \to 4^+$	0.2115	4.5585	1.20×10^{-1}		3.98×10^{-2}	3.87×10^{-1}
	$0^+ \to 1^-$	0.2537	4.5163	3.01×10^{-2}		5.87×10^{-1}	9.45×10^{-1}
	$0^+ \to 3^-$	0.3215	4.4485	9.74×10^{-4}		2.07×10^{-2}	1.11×10^{-1}
	$0^+ \to 6^+$	0.4165	4.3535	8.03×10^{-6}		4.25×10^{-5}	1.37×10^{-3}
	$0^+ \to 5^-$	0.4463	4.3237	1.03×10^{-5}		1.25×10^{-4}	2.21×10^{-3}
	$0^+ \to 0^+$	0.8246	3.9454	3.41×10^{-6}		6.76×10^{-6}	1.62×10^{-5}
	$0^+ \to 2^+$	0.8737	3.8963	1.19×10^{-4}		4.67×10^{-7}	3.76×10^{-6}
^{232}Th	$0^+ \to 0^+$	0	4.0816	7.83×10^{1}	−0.083	9.57×10^{1}	8.70×10^{1}
	$0^+ \to 2^+$	0.0638	4.0178	2.17×10^{1}		4.26	1.28×10^{1}
	$0^+ \to 4^+$	0.2047	3.8769	6.91×10^{-2}		1.65×10^{-2}	1.65×10^{-1}
Standard Deviation σ (for all states, including the ground-state)						0.749	0.973
σ (for excited states of even parity)						0.876	0.821
σ (for excited states of odd parity)						0.806	1.376

enhancement is noticed for the decay modes from some even-even Ra, Th, and U isotopes to low lying asymmetry states of negative parity (1^-, 3^-) of their daughter nuclei, relative to the corresponding decay modes to symmetric (4^+) states. This is observed for the decays leading to Rn, Ra, and Th daughter nuclei with $N_d = 132$, 134, and 136, and with a little enhanced intensity for those leading to $N_d = 130$ and 138. This opposes the reported additional hindrance for such decay modes between states of different parity, relative to those of the same parity. The indicated enhancement appears as a relative increase in the observed branching ratios and consequently a decrease in the corresponding partial half-lives. We found that this observed enhancement is independent of the change in T_α due to the change of the energy of the involved states, or the variation in the transferred angular momentum. Generally, the largest number of partial decay modes to various states of the daughter nucleus appears for the decays leading to $N_d = 130$–140. The major fraction of the α-branching ratio appear of course for the decay modes to the ground 0^+ state then to the first 2^+ low lying state. The largest branching ratios to the asymmetric 1^- and 3^- states, relative to those involving symmetric 4^+ states, are obtained for the decays to the Ra ($N = 134, 136, 138$) isotopes, followed by the decay modes to 1^- state in the Th ($N = 134$–140) then to Rn ($N = 134, 136$) isotopes, or those to 3^- state in the Rn ($N = 132$–136) then to Th ($N = 136, 138$) isotopes. The indicated enhancement is linked to the evolution of the octupole collectivity and the associated static octupole deformation of the actinides with $N \geqslant 134$.

The calculated branching ratios are compared with the observed values for the α-decay modes from the ground states of the even-even $^{222–232}$Th, ^{222,224,226}Ra, ^{228,232}U, and

TABLE II. The same as Table I but for Ra, U, and Pu isotopes.

Parent	Transition	E_{ex} (MeV)	Q_α (MeV)	B.R. exp (%)	β_3	B.R. calc (%)	
						with H_ℓ	without H_ℓ
^{222}Ra	$0^+ \to 0^+$	0	6.6780	9.69×10^{1}	−0.139	9.93×10^{1}	9.77×10^{1}
	$0^+ \to 2^+$	0.3243	6.3537	3.06		6.98×10^{-1}	2.29
	$0^+ \to (4^+)$	0.6531	6.0249	4.31×10^{-3}		1.70×10^{-3}	1.84×10^{-2}
	$0^+ \to (3^-)$	0.7969	5.8811	4.31×10^{-3}		1.28×10^{-3}	7.63×10^{-3}
	$0^+ \to (3^-)$	0.8402	5.8378	4.31×10^{-3}		2.85×10^{-4}	4.62×10^{-3}
^{224}Ra	$0^+ \to 0^+$	0	5.7889	9.49×10^{1}	−0.125	9.91×10^{1}	9.70×10^{1}
	$0^+ \to 2^+$	0.2410	5.5479	5.06		8.92×10^{-1}	2.91
	$0^+ \to 4^+$	0.5337	5.2552	7.10×10^{-3}		1.51×10^{-3}	1.63×10^{-2}
	$0^+ \to 1^-$	0.6454	5.1435	7.60×10^{-3}		1.08×10^{-2}	1.94×10^{-2}
	$0^+ \to (3^-)$	0.6630	5.1259	3.01×10^{-3}		9.80×10^{-4}	5.80×10^{-3}
^{226}Ra	$0^+ \to 0^+$	0	4.8706	9.38×10^{1}	−0.125	9.91×10^{1}	9.71×10^{1}
	$0^+ \to 2^+$	0.1862	4.6844	6.16		8.72×10^{-1}	2.84
	$0^+ \to 4^+$	0.4484	4.4222	6.50×10^{-3}		7.80×10^{-4}	8.42×10^{-3}
	$0^+ \to 1^-$	0.6007	4.2699	10^{-3}		1.65×10^{-3}	2.94×10^{-3}
	$0^+ \to 3^-$	0.6355	4.2351	2.70×10^{-4}		9.43×10^{-5}	5.59×10^{-4}
^{228}U	$0^+ \to 0^+$	0	6.8030	7.00	−0.153	8.99×10^{1}	7.59×10^{1}
	$0^+ \to 2^+$	0.0980	6.7050	2.88×10^{1}		6.27	1.76×10^{1}
	$0^+ \to (1^-)$	0.2460	6.5570	6.59×10^{-1}		3.70	5.70
	$0^+ \to 4^+$	0.2800	6.5230	5.66×10^{-1}		9.20×10^{-2}	8.56×10^{-1}
^{232}U	$0^+ \to 0^+$	0	5.4136	6.81×10^{1}	−0.111	9.22×10^{1}	7.78×10^{1}
	$0^+ \to 2^+$	0.0578	5.3558	3.15×10^{1}		7.29	2.05×10^{1}
	$0^+ \to 4^+$	0.1869	5.2267	3.00×10^{-1}		1.07×10^{-1}	9.93×10^{-1}
	$0^+ \to 1^-$	0.3279	5.0857	6.16×10^{-3}		3.86×10^{-1}	5.92×10^{-1}
	$0^+ \to 6^+$	0.3779	5.0357	5.10×10^{-5}		2.66×10^{-4}	8.22×10^{-3}
	$0^+ \to 3^-$	0.3960	5.0176	4.80×10^{-5}		1.70×10^{-2}	8.68×10^{-2}
	$0^+ \to 5^-$	0.5191	4.8945	5.60×10^{-5}		1.56×10^{-4}	2.65×10^{-3}
	$0^+ \to 0^+$	0.8314	4.5822	2.09×10^{-5}		8.59×10^{-5}	1.97×10^{-4}
	$0^+ \to 2^+$	0.8746	4.5390	3.90×10^{-6}		6.97×10^{-6}	5.30×10^{-5}
^{230}Pu	$0^+ \to 0^+$	0	7.1800	8.10×10^{1}	−0.139	9.05×10^{1}	7.41×10^{1}
	$0^+ \to 2^+$	0.0590	7.1210	1.90×10^{1}		9.53	2.59×10^{1}
Standard Deviation σ (for all states, including the ground-state)						0.800	0.967
σ (for excited states of even parity)						0.672	0.796
σ (for excited states of odd parity)						1.187	1.447

^{230}Pu isotopes, to the ground state and to the different low-lying excited states of their daughter nuclei. We found that the estimated branching ratio for the decay modes to the states of negative parity increases with considering the daughter deformations including the octupole deformations. Also, considering the hindrance in the spectroscopic preformation factor corresponding to the unfavored decay modes to the various higher excited states of the daughter nucleus is important to reproduce the observed branching ratios.

[1] P. D. Cottle and D. A. Bromley, Phys. Lett. B **182**, 129 (1986).

[2] G. A. Leander and R. K. Sheline, Nucl. Phys. A **413**, 375 (1984).

[3] A. M. Y. El-Lawindy, J. D. Burrows, P. A. Butler, J. R. Cresswell, V. Holliday, G. D. Jones, R. Tanner, R. Wadsworth, D. L. Watson, K. A. Connell, J. Simpson, C. Lauterbach, and J. R. Mines, J. Phys. G: Nucl. Phys. **13**, 93 (1987).

[4] P. A. Butler, L. P. Gaffney, P. Spagnoletti, K. Abrahams, M. Bowry, J. Cederkäll, G. de Angelis, H. De Witte, P. E. Garrett, A. Goldkuhle, C. Henrich, A. Illana, K. Johnston, D. T. Joss, J. M. Keatings, N. A. Kelly, M. Komorowska, J. Konki, T. Kröll, M. Lozano, B. S. Nara Singh, D. O'Donnell, J. Ojala, R. D. Page, L. G. Pedersen, C. Raison, P. Reiter, J. A. Rodriguez, D. Rosiak, S. Rothe, M. Scheck, M. Seidlitz, T. M. Shneidman, B. Siebeck, J. Sinclair, J. F. Smith, M. Stryjczyk, P. Van Duppen, S. Vinals, V. Virtanen, N. Warr, K. Wrzosek-Lipska, and M. Zielińska, Phys. Rev. Lett. **124**, 042503 (2020).

[5] H. J. Daley and B. R. Barrett, Nucl. Phys. A **449**, 256 (1986).

[6] A. K. Jain, R. K. Sheline, P. C. Sood, and K. Jain, Rev. Mod. Phys. **62**, 393 (1990).

[7] P. D. Cottle, Phys. Rev. C **42**, 1264 (1990).

[8] P. Möller, A. J. Sierk, T. Ichikawa, and H. Sagawa, At. Data Nucl. Data Tables **109–110**, 1 (2016).

[9] W. M. Seif and H. Anwer, Nucl. Phys. A **975**, 77 (2018).

[10] M. Beckers, C. Müller-Gatermann, A. Blazhev, T. Braunroth, A. Dewald, C. Fransen, A. Goldkuhle, L. Kornwebel, J.

Litzinger, F. von Spee, and K.-O. Zell, Phys. Rev. C **102**, 014324 (2020).
[11] S. Chopra, Hemdeep, P. Kaushal, and R. K. Gupta, Phys. Rev. C **98**, 041603(R) (2018).
[12] M. Ismail, W. M. Seif, and M. M. Botros, Nucl. Phys. A **828**, 333 (2009).
[13] M. Ismail, W. M. Seif, and M. M. Botros, Int. J. Mod. Phys. E **25**, 1650026 (2016).
[14] P. A. Butler and W. Nazarewicz, Rev. Mod. Phys. **68**, 349 (1996).
[15] M. Ismail and W. M. Seif, Nucl. Phys. A **872**, 25 (2011).
[16] M. Ismail and W. M. Seif, Phys. Rev. C **81**, 034607 (2010).
[17] M. Ismail and W. M. Seif, Int. J. Mod. Phys. E **22**, 1350010 (2013).
[18] J. Zhao, T. Nikšić, D. Vretenar, and S.-G. Zhou, Phys. Rev. C **99**, 014618 (2019).
[19] W. M. Seif, Nucl. Phys. A **767**, 92 (2006).
[20] W. M. Seif, J. Phys. G: Nucl. Part. Phys. **30**, 1231 (2004).
[21] J. Blons, Nucl. Phys. A **502**, 121 (1989).
[22] M. Csatlós, A. Krasznahorkay, P. G. Thirolf, D. Habs, Y. Eisermann, T. Faestermann, G. Graw, J. Gulyás, M. N. Harakeh, R. Hertenberger, M. Hunyadi, H. J. Maier, Z. Máté, O. Schaile, and H.-F. Wirth, Phys. Lett. B **615**, 175 (2005).
[23] K. Nomura, R. Rodríguez-Guzmán, L. M. Robledo, J. E. García-Ramos, and N. C. Hernández, Phys. Rev. C **104**, 044324 (2021).
[24] A. V. Afanasjev, H. Abusara, and S. E. Agbemava, Phys. Scr. **93**, 034002 (2018).
[25] R. K. Gupta, M. Balasubramaniam, R. Kumar, N. Singh, M. Manhas, and W. Greiner, J. Phys. G: Nucl. Part. Phys. **31**, 631 (2005).
[26] S. Jain, M. K. Sharma, and R. Kumar, Phys. Rev. C **101**, 051601(R) (2020).
[27] A. Adel, V. A. Rachkov, A. V. Karpov, A. S. Denikin, M. Ismail, W. M. Seif, and A. Y. Ellithi, Nucl. Phys. A **876**, 119 (2012).
[28] A. M. Stefanini, L. Corradi, A. M. Vinodkumar, Y. Feng, F. Scarlassara, G. Montagnoli, S. Beghini, and M. Bisogno, Phys. Rev. C **62**, 014601 (2000).
[29] W. M. Seif, Phys. Rev. C **91**, 014322 (2015).
[30] M. D. Sun, Z. Liu, T. H. Huang, W. Q. Zhang, A. N. Andreyev, B. Ding, J. G. Wang, X. Y. Liu, H. Y. Lu, D. S. Hou, Z. G. Gan, L. Ma, H. B. Yang, Z. Y. Zhang, L. Yu, J. Jiang, K. L. Wang, Y. S. Wang, M. L. Liu, Z. H. Li, J. Li, X. Wang, A. H. Feng, C. J. Lin, L. J. Sun, N. R. Ma, W. Zuo, H. S. Xu, X. H. Zhou, G. Q. Xiao, C. Qi, and F. S. Zhang, Phys. Lett. B **800**, 135096 (2020).
[31] W. M. Seif, M. M. Botros, and A. I. Refaie, Phys. Rev. C **92**, 044302 (2015).
[32] W. M. Seif, A. I. Refaie, and M. M. Botros, Indian J. Phys. **92**, 393 (2018).
[33] B. M. Musangu, A. H. Thibeault, T. H. Richards, E. H. Wang, J. H. Hamilton, C. J. Zachary, J. M. Eldridge, A. V. Ramayya, Y. X. Luo, J. O. Rasmussen, G. M. Ter-Akopian, Y. T. Oganessian, and S. J. Zhu, Phys. Rev. C **101**, 034610 (2020).
[34] I. Ahmad, J. P. Greene, F. G. Kondev, S. Zhu, M. P. Carpenter, R. V. F. Janssens, R. A. Boll, J. G. Ezold, S. M. Van Cleve, and E. Browne, Phys. Rev. C **87**, 054328 (2013).
[35] D. Ni and Z. Ren, Phys. Rev. C **81**, 064318 (2010).
[36] D. Ni and Z. Ren, Phys. Rev. C **83**, 067302 (2011).
[37] R. J. Poynter, P. A. Butler, N. Clarkson, D. Cline, K. A. Connell, R. A. Cunningham, L. Goettig, T. H. Hoare, J. R. Hughes, N. S. Jarvis, G. D. Jones, S. Juutinen, S. M. Mullins, C. N. Pass, J. Simpson, R. Wadsworth, D. L. Watson, and C. A. White, Phys. Lett. B **232**, 447 (1989).
[38] A. Adel and T. Alharbi, Phys. Rev. C **92**, 014619 (2015).
[39] A. Adel and T. Alharbi, Nucl. Phys. A **975**, 1 (2018).
[40] C. Xu and Z. Ren, Phys. Rev. C **74**, 014304 (2006).
[41] D. Ni and Z. Ren, Phys. Rev. C **86**, 054608 (2012).
[42] K. P. Santhosh and J. G. Joseph, Phys. Rev. C **86**, 024613 (2012).
[43] W. M. Seif and A. Adel, Phys. Rev. C **99**, 044311 (2019).
[44] M. Ismail, W. M. Seif, A. Adel, and A. Abdurrahman, Nucl. Phys. A **958**, 202 (2017).
[45] M. Ismail, A. Y. Ellithi, M. M. Botros, and A. Adel, Phys. Rev. C **81**, 024602 (2010).
[46] G. G. Adamian, N. V. Antonenko, R. V. Jolos, Y. V. Palchikov, W. Scheid, and T. M. Shneidman, Phys. Rev. C **69**, 054310 (2004).
[47] C. Xu and Z. Ren, Nucl. Phys. A **753**, 174 (2005).
[48] S. N. Kuklin, T. M. Shneidman, G. G. Adamian, and N. V. Antonenko, Eur. Phys. J. A **48**, 112 (2012).
[49] W. M. Seif and A. S. Hashem, J. Phys. G: Nucl. Part. Phys. **47**, 085103 (2020).
[50] W. M. Seif and A. Abdurrahman, Chin. Phys. C **42**, 014106 (2018).
[51] M. Ismail, W. M. Seif, and W. M. Tawfik, Indian J. Phys. **96**, 875 (2022).
[52] W. M. Seif and L. H. Amer, Nucl. Phys. A **969**, 254 (2018).
[53] A. Adel and A. R. Abdulghany, Phys. Scr. **96**, 125314 (2021).
[54] N. G. Kelkar and H. M. Castañeda, Phys. Rev. C **76**, 064605 (2007).
[55] F. Stancu and D. M. Brink, Nucl. Phys. A **270**, 236 (1976).
[56] E. Chabanat, P. Bonche, P. Haensel, J. Meyer, and R. Schaeffer, Nucl. Phys. A **635**, 231 (1998).
[57] W. M. Seif and A. S. Hashem, Chin. Phys. C **42**, 064104 (2018).
[58] V. Y. Denisov and W. Nörenberg, Eur. Phys. J. A **15**, 375 (2002).
[59] W. M. Seif and H. Mansour, Int. J. Mod. Phys. E **24**, 1550083 (2015).
[60] S. E. Agbemava, A. V. Afanasjev, and P. Ring, Phys. Rev. C **93**, 044304 (2016).
[61] J. M. Yao, E. F. Zhou, and Z. P. Li, Phys. Rev. C **92**, 041304(R) (2015).
[62] K. Nomura, D. Vretenar, T. Nikšić, and B.-N. Lu, Phys. Rev. C **89**, 024312 (2014).
[63] L. P. Gaffney, P. A. Butler, M. Scheck, A. B. Hayes, F. Wenander, M. Albers, B. Bastin, C. Bauer, A. Blazhev, S. Bönig, N. Bree, J. Cederkäll, T. Chupp, D. Cline, T. E. Cocolios, T. Davinson, H. De Witte, J. Diriken, T. Grahn, A. Herzan, M. Huyse, D. G. Jenkins, D. T. Joss, N. Kesteloot, J. Konki, M. Kowalczyk, T. Kröll, E. Kwan, R. Lutter, K. Moschner, P. Napiorkowski, J. Pakarinen, M. Pfeiffer, D. Radeck, P. Reiter, K. Reynders, S. V. Rigby, L. M. Robledo, M. Rudigier, S. Sambi, M. Seidlitz, B. Siebeck, T. Stora, P. Thoele, P. Van Duppen, M. J. Vermeulen, M. von Schmid, D. Voulot, N. Warr, K. Wimmer, K. Wrzosek-Lipska, C. Y. Wu, and M. Zielinska, Nature **497**, 199 (2013).
[64] K. Nomura, D. Vretenar, and B.-N. Lu, Phys. Rev. C **88**, 021303(R) (2013).
[65] L. M. Robledo and P. A. Butler, Phys. Rev. C **88**, 051302(R) (2013).
[66] L. M. Robledo, M. Baldo, P. Schuck, and X. Viñas, Phys. Rev. C **81**, 034315 (2010).

[67] P. Möller, R. Bengtsson, B. G. Carlsson, P. Olivius, T. Ichikawa, H. Sagawa, and A. Iwamoto, At. Data Nucl. Data Tables **94**, 758 (2008).
[68] G. Li-Sheng, M. Jie, and T. Hiroshi, Chin. Phys. Lett. **24**, 1865 (2007).
[69] J. F. C. Cocks, D. Hawcroft, N. Amzal, P. A. Butler, K. J. Cann, P. T. Greenlees, G. D. Jones, S. Asztalos, R. M. Clark, M. A. Deleplanque, R. M. Diamond, P. Fallon, I. Y. Lee, A. O. Macchiavelli, R. W. MacLeod, F. S. Stephens, P. Jones, R. Julin, R. Broda, B. Fornal, J. F. Smith, T. Lauritsen, P. Bhattacharyya, and C. T. Zhang, Nucl. Phys. A **645**, 61 (1999).
[70] J. L. Egido and L. M. Robledo, Nucl. Phys. A **494**, 85 (1989).
[71] W. Nazarewicz, P. Olanders, I. Ragnarsson, J. Dudek, G. A. Leander, P. Möller, and E. Ruchowsa, Nucl. Phys. A **429**, 269 (1984).
[72] H. J. Wollersheim, H. Emling, H. Grein, R. Kulessa, R. S. Simon, C. Fleischmann, J. de Boer, E. Hauber, C. Lauterbach, C. Schandera, P. A. Butler, and T. Czosnyka, Nucl. Phys. A **556**, 261 (1993).
[73] F. K. McGowan, C. E. Bemis, W. T. Milner, J. L. C. Ford, R. L. Robinson, and P. H. Stelson, Phys. Rev. C **10**, 1146 (1974).
[74] Computer code NUDAT 3.0, nuclear structure and decay data, https://www.nndc.bnl.gov/nudat3/.